Flow structure generated by laser-induced blast wave propagation through the boundary layer of a flat plate

Takahiro Ukai*

Institute of Fluid Science, Tohoku University, 2-1-1 Katahira, Aoba-ku, Sendai, Miyagi 980-8577, Japan

Konstantinos Kontis

University of Glasgow, School of Engineering, Glasgow, G12 8QQ, UK

Leichao Yang

National University of Defence Technology, Changsha, 410073, P.R. China

Corresponding author: *Takahiro Ukai

email: *ukai@edge.ifs.tohoku.ac.jp*

Telephone: + 81-22-217-5257

Abstract:

Laser energy deposition generates localised flow structures that can be used as flow control devices in high-speed flows. In the present study, the interaction between a laser-induced blast wave and an incoming laminar boundary layer on a flat plate was experimentally investigated at a Mach 5 flow with three different unit Reynolds numbers. A hemispherical laser-induced blast wave (LIBW) is induced by focusing a 532 nm pulsed Nd:YAG laser beam on the surface of the plate. The hemispherical shaped fore wave front of the LIBW is locally transformed to an oblique shape, which results in a laser-induced oblique shock wave (LIOSW). As LIOSW propagates through the laminar boundary layer increases its thickness. With laser energy deposition near the leading edge of the flat plate, the LIOSW interacts and influences the leading edge shock wave (LSW). This interaction could contribute to the modulation of the LSW in scramjet intakes. A weak shock limb generated at the shape transition point of the LIBW or thermal spot due to laser-induced gas breakdown causes the boundary layer perturbation. The geometrical pattern produced due to the interaction between the LIOSW and the disturbed boundary layer remains similar to itself as it grows with time as well as at different local Reynolds numbers, 2.2×10^5 to 5.7×10^5.

Keywords: Laser energy deposition; Self-similarity; Shock-boundary layer interaction; Flow control

1. Introduction

Laser energy deposition is an emerging technique to improve the aerodynamic performance of high-speed vehicles, and it has potential for various applications such as drag reduction [1, 2], shock wave modification [3, 4], and a controllable perturbation device for boundary layer transition studies [5]. Laser energy deposition can improve scramjet engine efficiency, thereby enabling the high-speed flying vehicles to operate at a wide range of Mach numbers. Scramjet engine efficiency deteriorates at an off-design flight Mach number by modulating the leading-edge shock because shock waves impinging within the engine inlet at a certain angle can only be achieved at a predetermined flight Mach number [6]. A numerical work by Macheret *et al.* [7] suggests that energy addition can be used to increase efficiency and performance at off-design flight Mach numbers. Drag reduction is directly related to more efficient transportation and less emission of harmful gases. When considering energy deposition upstream of a blunt body at a Mach 5 freestream flow, the bow shock wave interaction with the low density spot generated by the energy deposition, induces counter rotating vortices due to the baroclinic instability, which interact with the boundary layer of the blunt body contributing to drag reduction [8].

Understanding shock wave boundary layer interaction (SWBLI) is important for the improvement of aerodynamic performance. Complex flow features, such as: impinging oblique shock waves, normal shock wave reflections, and ramp flows are all present in a high-speed vehicle even without laser energy deposition. Laser energy deposition induces a blast wave and low density thermal spot, which result in complex SWBLI. Yan *et al.* [9] numerically investigated the effect of pulsed laser energy deposition on a normal shock-boundary layer interaction in the intake of an engine, and they showed that the normal shock wave moves towards upstream due to laser energy deposition. According to an experimental investigation [10], laser energy deposition can delay the shock induced separation over a flared cylinder. Tamba [11] and Iwakawa [12] showed that the boundary layer oscillation was significantly altered by the laser pulse duration.

The interaction of a blast wave with a boundary layer can induce many complicated flow features. In the present study, experiments were conducted to understand the interaction between the laser-induced blast wave and the incoming laminar boundary layer on a flat plate at a Mach 5 freestream flow. High-speed Schlieren photography was employed as the flow diagnostics technique. The laser induced blast wave was located at four different axial locations along the centreline of the plate. The flow structures due to the interaction were compared at three different unit Reynolds numbers.

2. Experimental setup

The experimental investigations were conducted at Mach 5 freestream flow with unit Reynolds numbers of 11.0×10^6, 13.0×10^6, and 14.6×10^6 m^{-1}, in an intermediate high supersonic blow-down wind tunnel. This wind tunnel consists of a high-pressure vessel, an electrical heater, a setting chamber, an axisymmetric Mach 5 nozzle, a test section, a diffuser, and a vacuum tank. The stable Mach 5 flow is maintained up to 7.5 seconds. The flow properties and wind tunnel configuration are presented in Refs. 13 to 15. The flow conditions are shown in Table 1. A flat plate model with its upper surface located on the nozzle centreline, was supported by a sting. The leading edge of the flat plate was sharp edge with the lower surface chamfered by 12°.

A Q-switched 532 nm pulsed Nd:YAG laser was used to deposit energy into a boundary layer of the plate. The laser beam (203 mJ/pulse; pulse width of approximately 4 ns) is introduced into the test section from the top window of the tunnel using a laser guide arm. In the present experiments, a combination of three lenses was used as suggested by Schmisseur *et al.* [5, 16]. The combination of the lenses enables focusing the laser beam into a smaller spot to obtain higher energy density even at the same laser beam energy level. The 25.4 mm concave lens with focal length of -100 mm expands the laser beam, then the 50 mm diameter convex lens with 250 mm focal length collimates the beam expansion. The laser beam is focused into a small spot at the focal position of the third convex lens. All of the optical lenses and the top window were coated with antireflective coating for a wavelength of 532 nm. The laser beam was focused on the flat plate at various streamwise positions along the model centreline. The laser focal positions were L = 10, 20, 30, and 40 mm downstream of the leading edge of the flat plate.

To visualise the unsteady phenomena, high-speed Schlieren photography with a standard Z-type optical arrangement was employed. The optical system consists of a 300 W continuous Xenon arc lamp for light source, two 203 mm parabolic mirrors with focal length of 1829 mm, and a high-speed camera (Photron, Fastcam SA-1.1). A horizontal rectangular slit in front of the light source creates a light spot that illuminates the first parabolic mirror. The light beam is then collimated by the first mirror and passes through a quartz side window. A second parabolic mirror reflects the collimated beam after the beam passes through the test section and the opposite quartz side window. A horizontal knife-edge is located at the focal point of the second parabolic mirror. The high-speed camera recorded the images at 90 kfps with an exposure time of 1 μs. An offset angle between the collimated light beam and the light path from the light source to the first/second mirrors was set at 10 degrees to prevent coma aberration.

3. Results and discussions

3.1 Flow structure without laser energy deposition

Figure 1 shows the flow structure over the flat plate without laser energy addition. A leading shock wave (LSW) generated from the leading edge of the flat plate is slightly curved in the vicinity of the leading edge due to viscus interaction. When hypersonic flow passes over the flat plate, the large displacement thickness of an initial boundary layer from a leading edge makes a virtual body. This virtual body refracts the incoming inviscid flow and consequently induces a slightly curved oblique shock wave [17, 18]. The weak compression waves are induced by a gap of the pressure taps along the model centre line, and would hardly affect the flow over the flat plate. The white region above the flat plate indicates the boundary layer growing in thickness gradually with distance. It is laminar based on the Reynolds numbers tested. To calculate the boundary layer thickness, a theoretical prediction is employed. Based on velocity distribution in a compressible laminar boundary layer on an adiabatic flat plate, thickness of the laminar boundary layer δ is predicted as;

$$\delta = \xi \cdot \sqrt{\frac{\nu_\infty \cdot x}{U_\infty}} \tag{1}$$

According to Schlichting [19], a non-dimensional parameter $\xi \approx 15.5$ for Mach 5 flow corresponds to a local velocity of $0.99U_\infty$. Where, U_∞, ν_∞, and x are the velocity, the kinematic viscosity, and the streamwise surface distance from the leading edge, respectively. The subscript "∞" refers to the freestream conditions. In the unit Reynolds numbers tested, from the Schlieren images, boundary layer thickness grows up to approximately 1 mm at the laser focal region of 40 mm from the leading edge (with the measurement uncertainty to be approximately +/- 10%). The theoretical predictions of boundary layer thickness, shown in Fig 2, indicate a thinner boundary layer. The relation between boundary layer thickness and laser-induced flow structure is discussed later.

3.2 Laser-induced flow structure

Laser energy deposition on the flat plate generates a blast wave that induces a localised flow perturbation. Figure 3 shows the typical Schlieren images of the laser focusing at 40 mm from the leading edge. The instant when the laser beam is focused on the plate is defined as $t = 0$ μs. The oblique shock wave observed over the plate is the leading shock wave (LSW). The bright region above the plate downstream of the LSW denotes plasma generation (Fig. 3 (a)). After the plasma generation, a hemispherical laser-induced blast wave (LIBW) propagates to surrounding and then is carried downstream by the freestream flow. The fore wave front of the LIBW has a higher-pressure magnitude

than that of the aft wave front. This is because the fore wave front of the LIBW propagates opposing the freestream flow direction. As shown in Fig. 3 (b), the fore wave front of the LIBW is clearly visible, which means a strong pressure change. On the other hand, the aft wave front which propagates towards downstream becomes weaker (Fig. 3 (b)) because of the same flow direction as the freestream.

The LIBW may increase boundary layer thickness. Due to interaction with the boundary layer, the hemispherical shaped fore wave front of the LIBW is locally transformed to the oblique shape, which results in the laser-induced oblique shock wave (LIOSW). The pressure behind the LIOSW that propagates through the boundary layer leads to the boundary layer development. Unfortunately, the Schlieren images do not ensure the fact that the boundary layer is separated or not due to the LIOSW. The starting point of the boundary layer development, which corresponds to the tip of the LIOSW, moves towards upstream (Fig. 3 (b-d)) because the pressure behind the LIOSW is kept developing upstream. As the pressure behind the LIOSW, which is propagating through the boundary layer, is getting closer to the local surface pressure upstream of the fore wave front, the tip of the LIOSW becomes weaker and gradually disappears.

The developed boundary layer is disturbed due to the thermal spot and/or the weak shock limb. Figure 4 shows the sketch of the laser-induced flow structure. There are two possibilities that the developed boundary layer is disturbed. Although it is difficult to observe the weak shock limb due to shock-shock interaction, the LIOSW would be reflected at the kink point. As a consequence, the weak shock limb is generated from the kink point. The weak shock limb that impinges on the boundary layer would lead to the perturbation of the boundary layer. A similar shock structure appears in shock-boundary layer interaction under high temperature condition in the shock tube experiments [20, 21]. In those shock tube experiments, a boundary layer is developed behind an incident shock wave and a high temperature region occurs behind a shock wave reflected from the end wall of the shock tube. Due to the interaction between the reflected shock and the boundary layer, a bifurcated shock wave is formed and then the aft bifurcated leg impinges on the boundary layer [21]. In the present experiment, with the high temperature gas occurring due to laser energy deposition, a similar shock structure can be observed. Another possibility is that the thermal spot generated by the laser-induced gas breakdown disturbs the boundary layer. The laser induced-gas breakdown event generates instantaneously locally a high temperature spot of the order of thousands Kelvin caused by gas vaporization and ablation on the wall surface [22]. The thermal spot supplies higher energy into the boundary layer at the instant of the gas breakdown event, which results in the perturbation of the boundary layer. The disturbed boundary layer remains and moves towards downstream even when the thermal spot disappears. However, the disturbed boundary layer would become gradually weaker.

The different flow velocities behind both the LIOSW and the LIBW results in the generation of a

slip line from the kink point (Fig. 3 (b)). As the direction of the slip line develops towards the surface of the flat plate, the streamlines across the fore wave front of the LIBW are refracted towards the wall surface. Since the LIBW expands hemispherically from the wall surface, it can allow the streamlines to bend towards the wall surface. The bent streamlines become parallel with the freestream across the aft wave front of the LIBW. The slip line gradually disappears (Fig. 3 (c) and (d)) due to either the same velocity magnitude behind both LIOSW and LIBW or weak gradients intensity due to a weak shock at later time.

3.3 Self-similarity of the laser-induced oblique shock wave

Geometrical pattern of the interaction between the LIOSW and the developed boundary layer is similar to itself in spite of different elapsed time and Reynolds numbers. Figure 5 shows the geometrical relation between the developed boundary layer and the LIOSW in a unit Reynolds number of 13.0×10^6 m^{-1}. The x-axis of these figures denotes the elapsed time from the laser focusing. The error bars show the standard deviation from four repetitions. The geometrical parameters h, l, and η are defined as the height from the wall surface to the kink point, the length from the tip of the LIOSW to the kink point, and the length from the tip of the LIOSW to the edge of the disturbed boundary layer, respectively (see, Fig. 4). To identify the tip of the LIOSW as well as the edge of the disturbed boundary layer, the image pixel intensity change by laser energy deposition was subtracted from a reference image pixel intensity. The reference image is the Schlieren image without laser energy deposition. The edge of the disturbed boundary layer can be observed on the wall surface at which a break of the white region appears (Fig. 3 (c)). The local Reynolds number Re_L, based on the initial laser focal distance L, is calculated as;

$$Re_L = \frac{U_\infty \cdot \rho_\infty \cdot L}{\mu_\infty} \tag{2}$$

Where, ρ_∞ and μ_∞ are density and viscosity, respectively. Figure 6 shows the comparison of the typical flow structure at the different laser focal positions. In the case of laser focusing at L = 10 mm (Fig. 6 (a)), which corresponds to $Re_L = 13.0 \times 10^4$ (Fig. 5), the LIOSW interacts with the LSW since the laser focal point is close to the leading edge. This interaction influences both the LIOSW and the LSW because the energy of the LIOSW is combined to the LSW, whereas the LIOSW does not interact with the LSW at all other laser focal points. Therefore, the geometrical parameter of the laser focal point at L = 10 mm is not considered to investigate self-similarity. As shown in Fig. 5 (a), the geometrical parameter h/η remains similar to itself as it grows with time except for the laser focal point at L = 10 mm. The geometrical parameter h/η is approximately 0.25 in unit Reynolds number of 13.0×10^6 m^{-1}. On the other hand, the geometrical parameter h/l (Fig. 5 (b)) decreases with time. Growth of the height

of the kink point is slower than the propagation of the tip of the LIOSW towards upstream. When considering the relation between the height of the kink point and boundary layer thickness without laser energy deposition, the height of the kink point becomes approximately four times as boundary layer thickness at elapsed time of 11 μs, then becomes approximately ten times at elapsed time of 55 μs. This is because growth of the height of the kink point is faster than that of boundary layer thickness.

Although the geometrical parameter h/l decreases linearly in proportion to the local Reynolds number, the geometrical parameter h/η is self-similar even as the local Reynolds numbers vary. Self-similarity related to the local Reynolds number is shown in Fig. 7. The solid lines denote the linear approximation by the least-squares method. In the present condition, it seems that the geometrical parameter h/η is independent of the local Reynolds number (Fig. 7 (a)). Even when the laser-induced flow field grows, the geometrical parameter h/η remains similar, whereas the geometrical parameter h/l changes in proportion to the local Reynolds number (Fig. 7 (b)). Additionally, the geometrical parameter h/l decreases as the laser-induced flow field grows; however, the gradient of the linear approximation curve at different time steps is similar to each other. Although self-similarity of laser-induced flow structure appeared at the present small range of the local Reynolds numbers, further numerical and experimental investigations are necessary to elucidate whether self-similarity appears in wider local Reynolds number including turbulent boundary layer conditions.

4. Conclusion

Laser energy deposition technique would contribute to a leading edge shock wave modulation in scramjet intakes at a wide range of flight Mach numbers. The focus of this study is the investigation of the laser-induced flow structure when laser energy deposits into an incoming laminar boundary layer on a flat plate. The experiments were conducted at Mach 5 freestream flow in the different unit Reynolds numbers of 11.0×10^6, 13.0×10^6, and 14.6×10^6 m^{-1}. A pulsed laser beam was focused on the surface of the flat plate at the different locations along the centreline (10, 20, 30, and 40 mm) from a leading edge. High-speed Schlieren photography was employed to investigate the induced unsteady phenomena.

The characteristics of the laser-induced gas breakdown in the present boundary layer condition is significantly different than that in a quiescent gas condition. Laser energy deposition on the wall surface generated a hemispherical laser-induced blast wave (LIBW). Thereafter, the hemispherical shaped fore wave front of the LIBW was locally transformed to the oblique shape, which results in the laser-induced oblique shock wave (LIOSW). Additionally, the fore wave front of the LIBW was apparently stronger than that of the aft wave front because the fore wave front propagated towards the opposite direction of the freestream. The LIOSW may increase a laminar boundary layer thickness due

to shock-boundary layer interaction (SWBLI). The developed boundary layer caused by the SWBLI was disturbed due to a weak shock limb and/or a thermal spot. The weak shock limb was generated from the kink point where the LIBW transformed to the LIOSW, and the thermal spot appeared due to laser-induced gas breakdown.

While the laser energy deposition technique has a potential to distort the leading edge shock wave, its effect significantly depends on the magnitude of the energy input at the freestream flow parameters. The strength of the LIOSW is varying as the distance from the leading-edge increases, becoming weaker further downstream. Hence to have a considerable oblique shock wave modulation for scramjet intakes for instance, substantial energy input may be required.

The laser-induced flow structure is related to itself. The geometrical parameter between the length/height of the LIOSW decreased in proportion to the local Reynolds number as well as growth of the laser-induced flow field. However, the interaction pattern between the LIOSW and the developed boundary layer remained self-similar as it grew with time as well as at different local Reynolds numbers from 2.2×10^5 to 5.7×10^5. Future work involves further investigation to understand self-similarity of laser-induced flow structure at a wider range of a local Reynolds numbers.

Acknowledgments

We would like to acknowledge our gratitude to Dr. Sriram Rengarajan, Mr. Adrian Walker and all the staff at the EPSRC Instruments Loan Pool.

Findings: This work has received funding from the European Union's Horizon 2020 research and innovation programme under the Marie Sklodowska-Curie Grant Agreement No. 654318 for conducting the analysis of this study.

References

[1] M.A.S. Minucci, P.G.P. Toro, A.C. Oliveira, J.B. Chanes Jr., A.L. Pereira, H.T. Nagamatsu, L.N. Myrabo, “Laser-supported directed-energy air spike in hypersonic,” *Journal of Spacecraft and Rockets* 42, 51-57, 2005.

[2] J.H. Kim, A. Matsuda, T. Sakai, A. Sasoh, “Wave drag reduction with acting spike induced by laser-pulse energy depositions,” *AIAA Journal* 49 (9), 2076-2078, 2011.

[3] D. Furukawa, Y. Aoki, A. Iwakawa, A. Sasoh, “Moderation of near-field pressure over a supersonic flight model using laser-pulse energy deposition,” *Physics of Fluid* 28, 051701, 2016.

[4] S.H. Zaidi, M.N. Shneider, R.B. Miles, “Shock-wave mitigation through off-body pulsed energy deposition,” *AIAA Journal* 42 (2), 326-331, 2004.

[5] J.D. Schmisseur, S.P. Schneider, S.H. Collicott, “Supersonic boundary-layer response to optically generated freestream disturbances,” *Experiments in Fluids* 33(2) 225-232, 2002.

[6] M.N. Shneider, S.O. Macheret, S.H. Zaidi, I.G. Girgis, R.B. Miles, "Virtual shapes in supersonic flow control with energy addition," *Journal of Propulsion and Power* 24(5), 900-915, 2008.

[7] S.O. Macheret, M.N. Shneider, R.B. Miles, "Scramjet inlet control by off-body energy addition: a virtual cowl," *AIAA Journal* 42(11), 2294-2302, 2004.

[8] Y. Ogino, N. Ohnishi, S. Taguchi, K. Sawada, “Baroclinic vortex influence on wave drag reduction induced by pulse energy deposition,” *Physics of Fluids* 22, 066102, 2009.

[9] H. Yan, D. Knight, R. Kandala, G. Candler, “Effect of a laser pulse on a normal shock,” *AIAA Journal* 45 (6), 1270-1280, 2007.

[10] T. Osuka, E. Erdem, N. Hasegawa, R. Majima, S. Yokota, A. Sasoh, K. Kontis, “Laser energy deposition effectiveness on shock-wave boundary-layer interactions over cylinder-flare combinations,” *Physics of Fluids* 26, 096103, 2014.

[11] T. Tamba, H.S. Pham, T. Shoda, A. Iwakawa, A. Sasoh, “Frequency modulation in shock wave-boundary layer interaction by repetitive-pulse laser energy deposition,” *Physics of Fluids* 27, 091704, 2015.

[12] A. Iwakawa, T. Shoda, H.S. Pham, T. Tamba, A. Sasoh, “Suppression of Low-Frequency Shock Oscillations over Boundary Layers by Repetitive Laser Pulse Energy Deposition,” *Aerospace* 3 (13), 2016.

[13] T. Ukai, H. Zare-Behtash, K. Kontis, L. Yang, E. Erdem, “Experimental investigation of surface flow pattern on truncated cones in Mach 5 flow: Influence of truncation ratio,” *Experimental Thermal and Fluid Science* 81, 396-405, 2017.

[14] E. Erdem, K. Kontis, “Numerical and experimental investigation of transverse injection flows,”

Shock Wave 20, 103-118, 2010.

[15] E. Erdem, K. Kontis, L. Yang, "Steady energy deposition at Mach 5 for drag reduction," *Shock wave* 23 (84) 258-1264, 2013.

[16] J.D. Schmisseur, S.H. Collicott, S.P. Schneider, "Laser-generated localized freestream perturbations in supersonic and hypersonic flows," *AIAA Journal* 38(4) 666-671, 2000.

[17] E.H. Hirschel, "Basics of aerothermodynamics; Second Revised Edition, Springer, 2015.

[18] J.D. Anderson Jr, "Hypersonic and high-temperature gas dynamics; Second Edition," AIAA education series, 2006.

[19] H. Schlichting, "Boundary layer theory," McGraw-Hill, 1960.

[20] L. Davies, "The interaction of the reflected shock with the boundary layer in a shock tube and its influence on the duration of hot flow in the reflected-shock tunnel, Part 1," C.P. No. 880, 1966.

[21] H. Mark, "The interaction of a reflected shock wave with the boundary layer in a shock tube," NACA TM 1418, 1958.

[22] R. Noll, "Laser-induced breakdown spectroscopy, Fundamentals and applications," Springer, 2012.

Figures

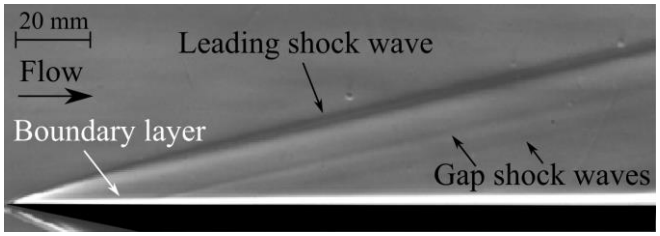

Figure 1: Schlieren image of the Mach 5 flow with Re_{unit} = 13.0 × 10^6 m^{-1} over the flat plate without laser energy addition.

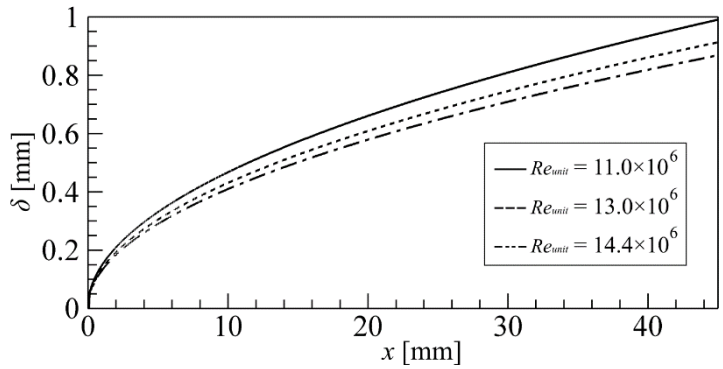

Figure 2: Theoretical prediction of the surface pressure distribution on the flat plate in Mach 5 flow.

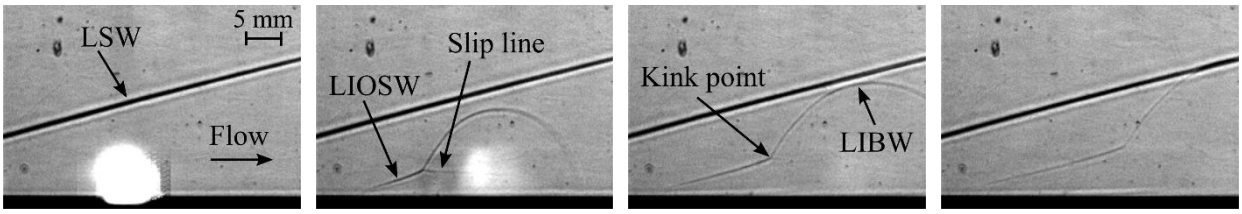

(a) t = 0 μs (b) t = 11 μs (c) t = 22 μs (d) t = 33 μs

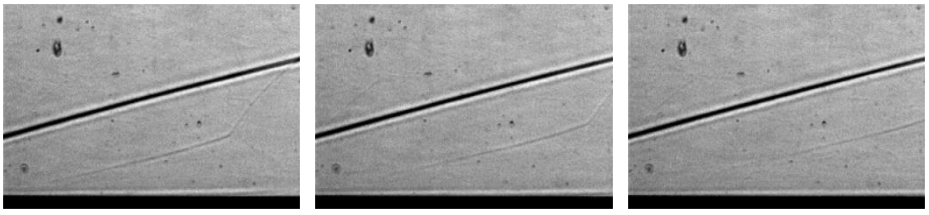

(e) t = 44 μs (f) t = 55 μs (g) t = 66 μs

Figure 3: Time-resolved Schlieren images of laser energy deposition on the flat plate at 40 mm from the leading edge. Unit Reynolds number is 13.0 × 10^6 m^{-1}.

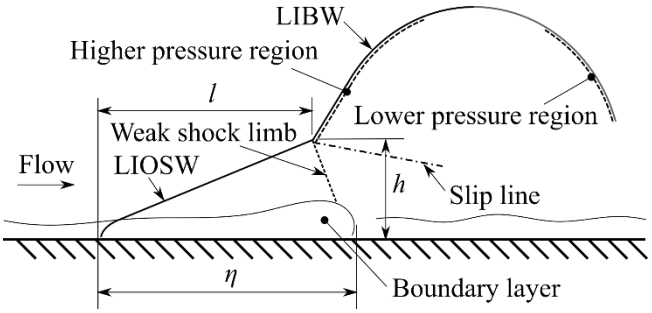

Figure 4: Induced flow structure due to laser energy deposition.

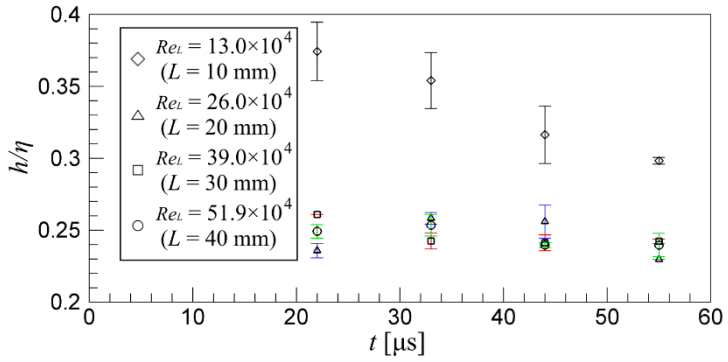

(a) h/η

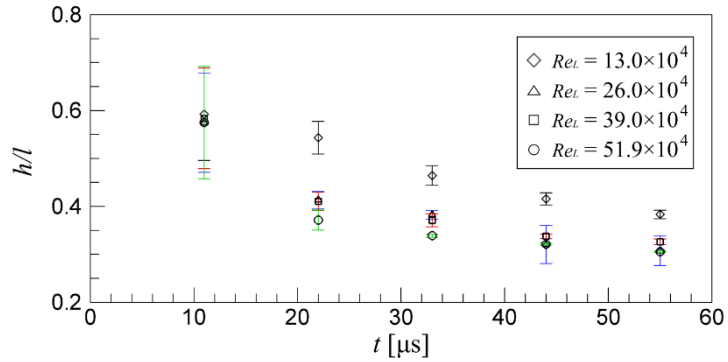

(b) h/l

Figure 5: (Color online) Geometrical relation between the developed boundary layer and the LIOSW in unit Reynolds number of 13.0×10^6 m^{-1}.

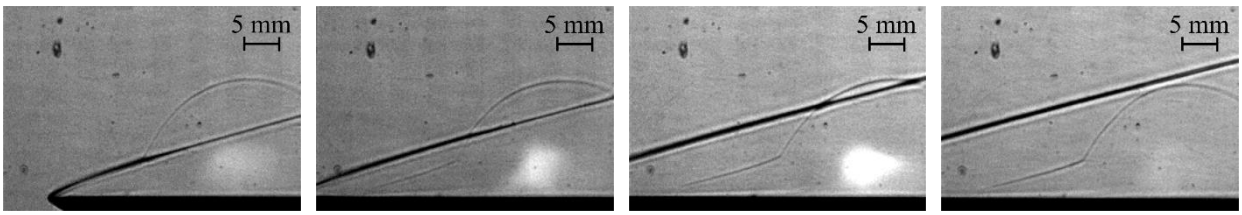

(a) L = 10 mm (b) L = 20 mm (c) L = 30 mm (d) L = 40 mm

Figure 6: Comparison of the typical flow structure at elapsed time of 22 μs at the different laser focal points in unit Reynolds number of 13.0×10^6 m^{-1}.

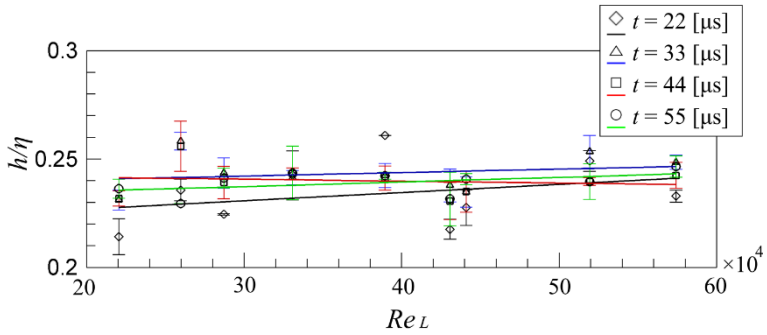

(a) h/η

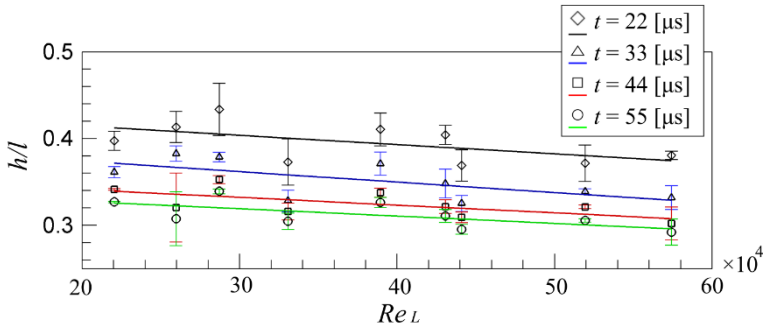

(b) h/l

Figure 7: (Color online) Self-similarity related to the local Reynolds number.

321 **Table**

322 Table 1 Experimental conditions.

Unit Reynolds number Re_{unit} [m^{-1}]	Total pressure P_t [kPa]	Total temperature T_t [K]	Freestream pressure P_∞ [kPa]	Mach number
11.0×10^6	547.75	372.3	1.03	5.0
13.0×10^6	640.62	375.5	1.23	5.0
14.4×10^6	719.9	375.5	1.36	5.0